ELSEVIER

International Journal of Refractory Metals & Hard Materials 18 (2000) 153–161

International Journal of
REFRACTORY METALS
& HARD MATERIALS

Advances in modern nitrogen-containing hardmetals and cermets

Limin Chen [a,*], Walter Lengauer [b], Klaus Dreyer [c]

[a] *Austrian Research Center, Seibersdorf, A-2444, Austria*
[b] *Institute for Chemical Technology of Inorganic Materials, Vienna University of Technology, Getreidemarkt 9/161, A-1060, Austria*
[c] *WIDIA GmbH, Munchener Str. 90, D-45145, Essen, Germany*

Received 22 December 1999; accepted 30 April 2000

Dedicated to Prof. Dr.-Techn. Dipl.-Ing. P. Ettmayer on the occasion of his 65th birthday

Abstract

Properties and performances of modern hardmetals and cermets can be significantly improved by introducing nitrogen (N) to optimise micro- and macro-structures. However, nitridation and de-nitridation complicate metallurgical reactions during sintering. By using SEM/EDS, XRD, DSC, DTA, mass spectrometer (MS) and dilatometer (DL), phase reactions, phase equilibria, melting points and sintering behaviours of WC–TiC–TiN–, WC–TiC–TiN–Co– and WC–TiCN–TaC/NbC–Co/Ni– alloys have been studied. Based on better understanding of the above systems related to sintering atmospheres, various new cutting tool materials with specially designed chemistries, micro- and macro-structures and properties have been prepared. The new materials can be classified as (1) cubic phase-free-layered surface (CFL) materials for substrates of coating tools; (2) graded materials with hard cermet surface and tough hardmetal core; (3) complex multi-laminated materials with graded compositions within each surface layer; and (4) TiN-based self-lubricated materials. The keys to obtain desired materials are to control metallurgical reactions during sintering and to design chemical compositions of the materials properly.

Keywords: Cemented carbides; Cermets; Cutting tools; Micro-structure; Thermal analysis

1. Introduction

The performance of cutting tools depends on both the bulk properties of the materials and the properties of the surface region. These properties are dependent on the chemical compositions and micro-structures. As early as 1970s, nitrogen was introduced into TiC–Ni–Mo cermet alloys to improve its performance by modifying the micro-structure especially the grain size of the hard particles [1–3]. The grain growth of the hard particles has been inhibited by the introduction of TiN into cermets. Modern cermets consist of TiC/TiN as main hard component and Co/Ni as binder. In addition, 20–40 mass% Mo_2C, WC, TaC, NbC and VC are usually added to improve the sinter ability and hot hardness. Accordingly, the micro-structures of cermets, whose hard particles often have ''core-rim'' structure are much more complex than those of relatively straightforward WC–Co hardmetals. The core is essentially un-dissolved TiCN and/or TiN. The rim is enriched in heavier elements W, Ta/Nb and Mo and has the same cubic crystal structure as the core. With increasing nitrogen content in cermets, the grain size of the hard particles and the thickness of the rim generally decrease. The performance of modern cermets to machine steels at high speed is as good as or even better than that of coated hardmetals [4].

Nitrogen also plays an important role as far as coated hardmetals are concerned. The micro-structure in the surface region of coated substrates has been modified by introducing nitrogen to develop a cobalt enriched, cubic-carbide free layer (CFL) [5–7]. The lifetime of coated hardmetals using CFL substrates can be significantly extended due to increased toughness beneath coating layers. In the mid 1990s functionally graded material (FGM) hardmetal was developed by sintering of TiCN–WC–Co/Ni under nitrogen atmosphere [8]. The FGM hardmetal consists of a high wear resistant cubic-carbide enriched surface layer, a tough core

* Corresponding author. Present address: SinterMet Inc., North Park Drive, West Hills Industrial Park, Kittanning, PA 16201-8883, USA. Tel.: +01-724-548-7631; fax: +01-724-545-1824.
E-mail address: limin.chen@sintermet.com (L. Chen).

0263-4368/00/$ - see front matter
PII: S0263-4368(00)00016-0

containing WC, cubic carbides/carbonitrides and Co/Ni binder, and an intermediate zone with graded compositions. The FGM hardmetal was reported to display better wear resistance and impact resistance compared to cermet and coated hardmetals. However, systematic studies of phase equilibria, metallurgical mechanisms and processing technologies of nitrogen-containing hardmetals and cermets have never been published. Therefore, a series of our recent research have been carried out [9,10]. In addition to the above-mentioned cermets, CFL and FGM, new nitrogen-containing hardmetals and cermets have been developed. This work presents part of our results.

2. Experiments

A series of samples different in composition were prepared to investigate TiC–TiN–WC hard phase system. The samples were made of well analysed TiC, TiN and WC powders, which were ball-milled for half-an-hour in Cyclohexane, dried and hot-pressed at 2300°C under 55 MPa in an inert Ar atmosphere. To obtain the thermodynamic equilibrium at 1500°C, the hot-pressed samples were annealed in an Ar atmosphere (1 bar) for 168 h. Then the Ar annealed samples were cut into plates, each about 2-mm thick for phase characterisation by XRD and SEM/EDS. To study the interaction of the WC–TiC–TiN hard phases with N_2, the Ar annealed samples were treated at 1500°C under different nitrogen pressure, 10 bar N_2 for 96 h and 30 bar N_2 for 66 h, respectively. Afterwards, the N_2 treated samples were examined by EPMA and SEM/EDS.

The melting behaviours of WC–TiC–TiN–33 wt% Co and WC–TiC–TiN–TaC–33 wt% Co alloys were investigated by DTA. By those compositions, the hard phases will not dissolve completely into liquid and the amount of the liquid phase is enough to give a DTA thermal signal. DTA was carried out in Al_2O_3 crucible under 700 mbar Ar (99.999%) atmosphere up to 1550°C. The heating and cooling rates for all specimens were 10°C/min. Several runs were performed by repeatedly heating and cooling each sample for four to six times. DTA samples were then observed by SEM/EDS.

Green compact samples with compositions of WC–TiC–TiN—10 wt% Co and WC–TiC–TiN–TaC/NbC—10 wt% Co/Ni were prepared by "state-of-the-art" industrial process. Melting behaviour, sintering behaviour and out-gas process were investigated by using different scanning calorimeter (DSC), dilatometer (DL) and mass spectrometer (MS), respectively. The out-gases of CO and N_2 during sintering were investigated by MS using an MF furnace with a silica tube attached to a high vacuum system. In the MF furnace a high-pressure interface was inserted between the recipient and the quadrupole mass spectrometer system in order to be able to characterise the sintering atmosphere at pressures in the mbar range. This is necessary because a He gas stream has to be used to elute the gases from the crucible into the MS system. A gas flow system together with a second pump was used to keep a constant pressure of 20 mbar. The ion fluxes of CO^+, N_2^+ and N^+ were recorded, calibrated against standard gas mixtures and introduced in a system of linear equations (because of the coincidence of N_2^+ and CO^+ at mass 28) to solve for the CO and N_2 concentrations.

In order to obtain materials featuring different micro- and macro-structures, sintering parameters especially sintering atmospheres (vacuum, Ar, H_2, CH_4 and N_2 from 50 mbar to 90 MPa) were studied. Sintered samples were examined by XRD, SEM/EDS and glow discharge spectrometer (GDS) afterwards. Experimental details were given in [9,10].

3. Results

3.1. Phase formation in the TiC–TiN–WC hard phase system

As shown in Fig. 1, two f.c.c. (Ti, W)(C, N) phases δ_1 and/or δ_2 were observed in the whole compositional range of the WC–TiC–TiN hard phase system. Since the composition of the two f.c.c. phases were quite similar, profile fitting with the Difpatan X-ray diffraction program had to be applied to identify the phases. In the composition region A, only one f.c.c. (Ti, W)(C, N)

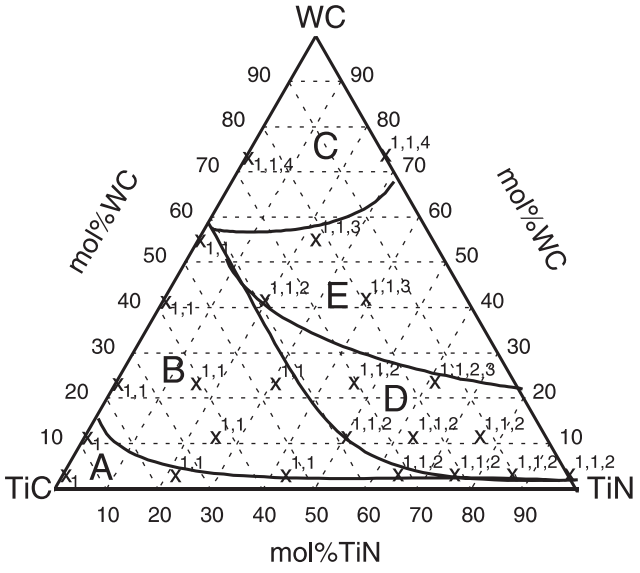

Fig. 1. Phases existence in the TiC–TiN–WC hard phase system after the Ar-annealing (1500°C, 168 h). The meaning of the numbers in the chart are: 1 – f.c.c.-(Ti, W)(C, N); 2 – b.c.c-W; 3 – hex-W_2C; 4 – hex-WC.

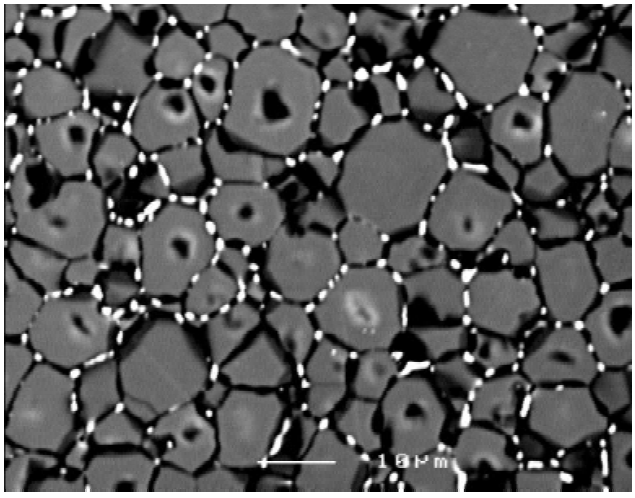

Fig. 2. SEM image of a hot-pressed (2300°C) and Ar annealed (1500°C, 168 h). (Ti, W)(C, N) sample; WC/TiC/TiN = 12/26/62 in mol%; magnification: 400×.

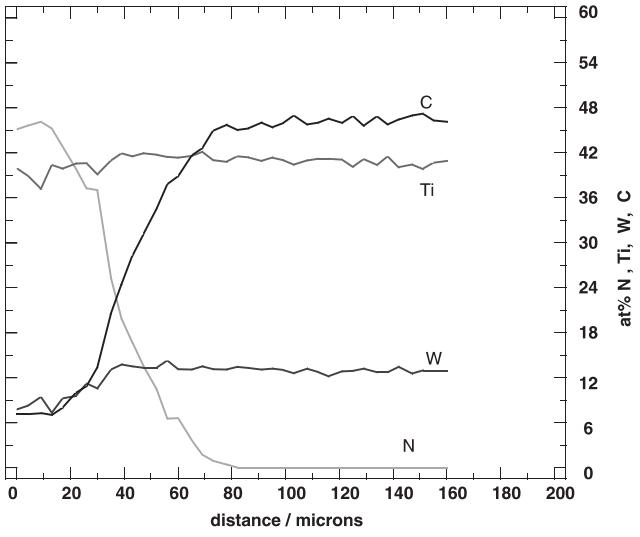

Fig. 3. Element distribution of the surface interaction zone of a (Ti, W)(C, N) sample after N_2 annealing at 1500°C and 30 bar N_2 (WC/TiC/TiN = 24/76/0 in mol%); measured by EPMA.

phase was observed. Two f.c.c. phases δ_1 and δ_2 were observed in the compositional region B. In the compositional regions C, D and E, hex-WC, b.c.c.-W and hex-W_2C, respectively, coexisted with δ_1 and δ_2.

Fig. 2 shows an example of the micro-structure of an alloy with a composition of WC/TiC/TiN = 12/26/62 in mol%. Since the composition of the sample is located in the D area of the TiC–TiN–WC system, three phases with different colours in the micro-structure – gray (δ_1), dark (δ_2) and white (b.c.c.-W) – were distinctly observed.

3.2. Interaction of TiC–TiN–WC alloys with N_2

Quaternary (Ti, W)(C, N) alloys will react with N_2 atmosphere at high temperatures. The element distributions across sample section show gradients of C, N and W (see Fig. 3). N concentration decreases while C and W concentrations rise with increasing distance from the sample surface. Depending on N_2 pressure, temperature and chemical composition, the quaternary (Ti, W)(C, N) alloys may decompose into two f.c.c. phases δ_1 and δ_2 and WC through

$$(\mathrm{Ti,\ W})(\mathrm{C,\ N}) + \mathrm{N_2} \rightarrow (\mathrm{Ti}_x,\ \mathrm{W}_{1-x})(\mathrm{C}_{x'},\ \mathrm{N}_{1-x'}) + (\mathrm{Ti}_y,\ \mathrm{W}_{1-y})(\mathrm{C}_{y'},\ \mathrm{N}_{1-y'}) + \mathrm{WC},$$

where $(\mathrm{Ti}_x,\ \mathrm{W}_{1-x})(\mathrm{C}_{x'},\ \mathrm{N}_{1-x'})$ is rich in Ti, and N and $(\mathrm{Ti}_y,\ \mathrm{W}_{1-y})(\mathrm{C}_{y'},\ \mathrm{N}_{1-y'})$ is rich in W and C. In micro-structure $(\mathrm{Ti}_x,\ \mathrm{W}_{1-x})(\mathrm{C}_{x'},\ \mathrm{N}_{1-x'})$ is darker than $(\mathrm{Ti}_y,\ \mathrm{W}_{1-y})(\mathrm{C}_{y'},\ \mathrm{N}_{1-y'})$. An example of the N_2 reacting surface zones is given in Fig. 4. It is evident that the dark gray $(\mathrm{Ti}_x,\ \mathrm{W}_{1-x})(\mathrm{C}_{x'},\ N_{1-x'})$ phase and the bright $(\mathrm{Ti}_y,\ \mathrm{W}_{1-y})(\mathrm{C}_{y'},\ \mathrm{N}_{1-y'})$ phase are located at the grain boundaries of the original (Ti, W)(C, N). WC phase

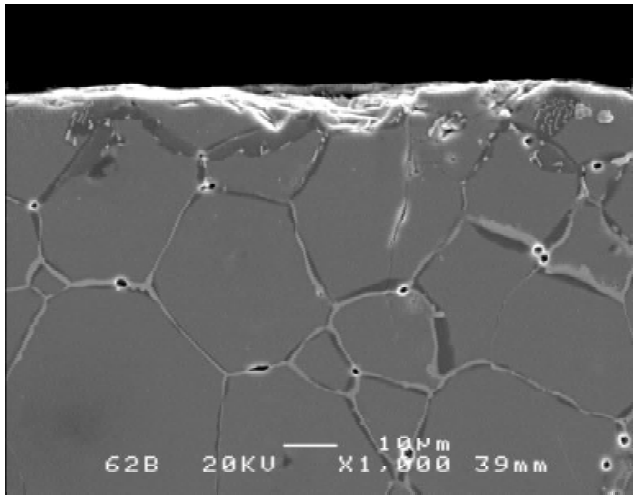

Fig. 4. SEM image of the surface interaction zone of a (Ti, W)(C, N) sample after N_2 annealing at 1500°C, 10 bar N_2; WC/TiC/TiN = 12/64/24 in mol%; magnification: 1000×.

(small white phase) was also seen at the grain boundary near surface (Fig. 4).

3.3. Melting behaviours of WC–TiC–TiN–Co– and WC–TiCN–TaC/NbC–Co/Ni– alloys

Fig. 5 summarises the melting point temperatures of 50 DTA alloys and 30 DSC alloys in the WC–TiC–TiN–Co system. Phase boundary between WC + (Ti, W)(C, N) + Co and (Ti, W)(C, N) + Co regions was determined by SEM/EDS and XRD. All alloys with compositions lying in the WC-existing region of WC + (Ti, W)(C, N) + Co have the same melting point temperature of

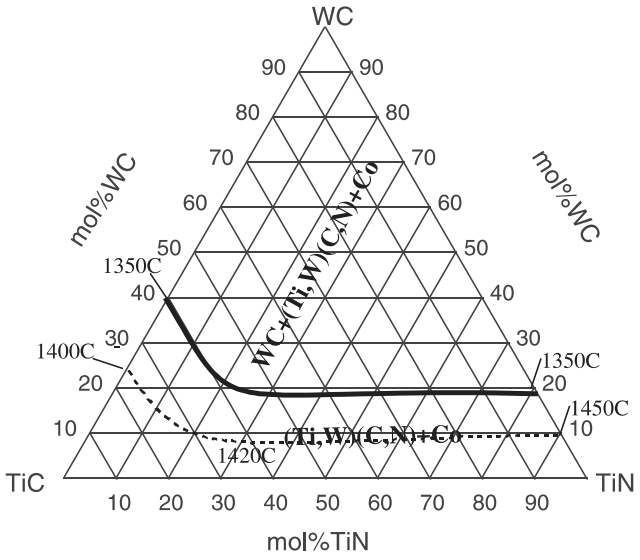

Fig. 5. Melting point temperatures and phase boundary in the WC–TiC–TiN–Co system. Alloys located in the WC + (Ti, W)(C, N) + Co region have the same melting point temperature of 1350°C.

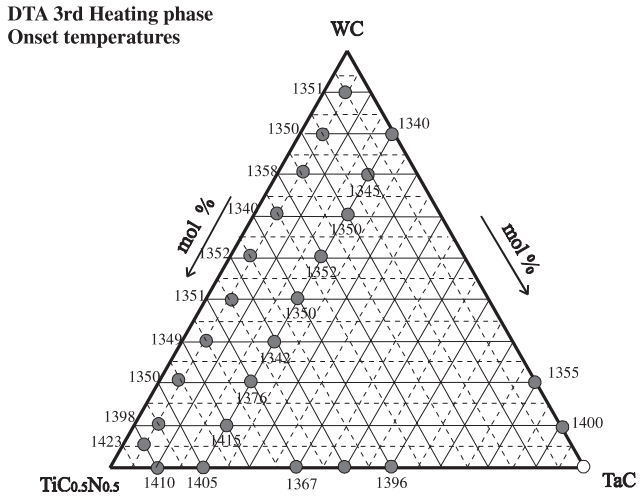

Fig. 6. Melting point temperatures in the $TiC_{0.5}N_{0.5}$–WC–TaC–Co system; number in the figure in °C.

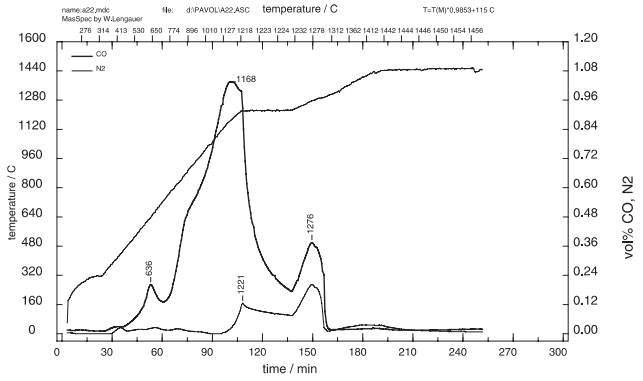

Fig. 7. CO and N_2 evolution of a sample measured by MS. The three different parts of CO evolution due to reduction can be clearly observed.

about 1350°C. The melting point temperatures of the alloys lying in the (Ti, W)(C, N) + Co region are 50–100°C higher than that of the alloys being located in the WC + (Ti, W)(C, N) + Co region. There is a temperature gradient of the melting points when alloy compositions shift from the WC + (Ti, W)(C, N) + Co region into the (Ti, W)(C, N) + Co region. Moreover, there is also a temperature gradient of the melting points when TiN/TiC ratio of the alloys in the (Ti, W)(C, N) + Co region increases (see dotted line in the Fig. 5).

The influence of TaC and TaC/NbC additives on the melting point temperatures of WC–TiC–TiN–Co alloys was investigated by DTA and DSC. No change of the melting point temperatures was found. Alloys containing more than 80 mol% WC have the same melting point temperature of about 1350°C as shown in Fig. 6.

In order to study the influence of Ni on the melting point temperatures, a WC–TiC–TiN–Co alloy and a WC–TiC–TiN–Co/Ni alloy were investigated by DSC. The two alloys have the same composition of the hard phase which is located in the WC-existing region. For the alloy containing Co/Ni binder the melting point temperature is 1400°C, which is about 50°C higher than that of the alloy containing only Co binder.

3.4. Metallurgical reactions during sintering

An example of metallurgical reactions during sintering is given in Fig. 7. The evolution of CO is much larger than that of N_2. Three parts of the evolution of CO were observed. The first CO peak arises around 600–700°C. This peak results from the reduction of the surface of the binder phase particles. The main CO peak located around 1100–1250°C is caused by the reduction of oxygen in the hard phase particles. At temperatures of 1250–1300°C, a small CO peak arises as result of the reduction of hard phase particles and the action of the liquid phase. If the powder compacts contain nitrogen, the main N_2 peak arises at almost the same position as the final CO peak. It can be seen that nitrogen evolution takes place shortly before the green compacts start to shrink drastically. Because of liquid phase formation, the CO and N_2 evolution stops and drops to almost the level of blank values. This is due to densification and plugging of the pores.

By combination of modern thermal analysis methods of DTA/DSC, DIL and MS, the metallurgical reactions during sintering are schematically summarised in Fig. 8. The evolution of CO from chemisorbed or chemically bonded oxygen on the surface of the powder particles, particularly on the surface of the titanium containing hard particles emerges around 900°C, peaks around

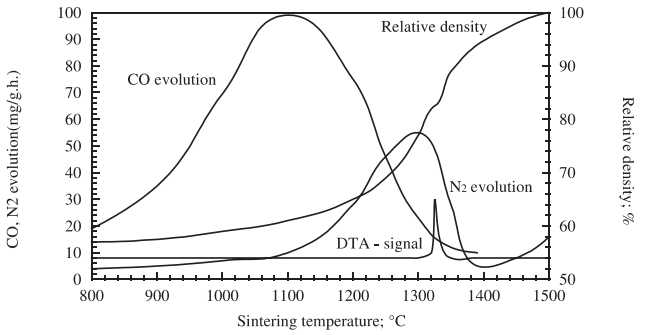

Fig. 8. Schematic illustration of the metallurgical reactions during sintering of nitrogen-containing hardmetals and cermets.

1100–1200°C and fades out at about 1250°C. The presence of Co/Ni binder greatly accelerates the evolution of CO and therefore improves the removal of the oxide layers from the powder particles. The evolution of nitrogen sets in at about 1200°C and has a very marked maximum at about 1300°C. With increasing temperature the rate of nitrogen evolution decreases and begins to gradually increase again only above 1500°C. With the onset of liquid phase formation at approximate 1350°C, nitrogen evolution drops drastically because of the shrinkage of the compacts. The formation of liquid phase appears not to be influenced by starting materials of either pre-alloyed quaternary carbonitrides or powder mixtures of TiC, TiN and WC. In the range of our experiments, even the stoichiometric factor x of the hard phase (Ti, W)(C, N)$_x$ ($x = 0.85$–1) did not influence the melting point temperatures very much.

Figs. 9 and 10 indicated that the more the nitrogen content in the hard phase particles, the higher is the temperature of the CO evolution. It can be understood considering the fact that the richer the hard phase is in carbon, the more readily the powder particles are reduced, – vice versa – the higher the nitrogen content is, the more sluggish the reduction reaction is to form CO. Figs. 11 and 12 show the temperatures of the main N_2 peaks arising from the interaction of liquid phase formation with the hard phase. The temperatures vary with the compositions of the hard phases in the TiC–TiN–WC system. The information of the CO and N_2 evolution is the key point to determine the type of the sintering atmosphere so as to obtain different micro- and macro-structures.

3.5. Micro-structure features of the bulk materials

WC–TiC–TiN–Co and WC–TiC/TiN–TaC/NbC–Co/Ni alloys with hard phase covering the whole composition range of WC–TiC–TiN system can be fully densified by the ''state-of-the-art'' industry processes. The micro-structure of the sintered alloy depends significantly on the composition of the WC–TiC–TiN hard

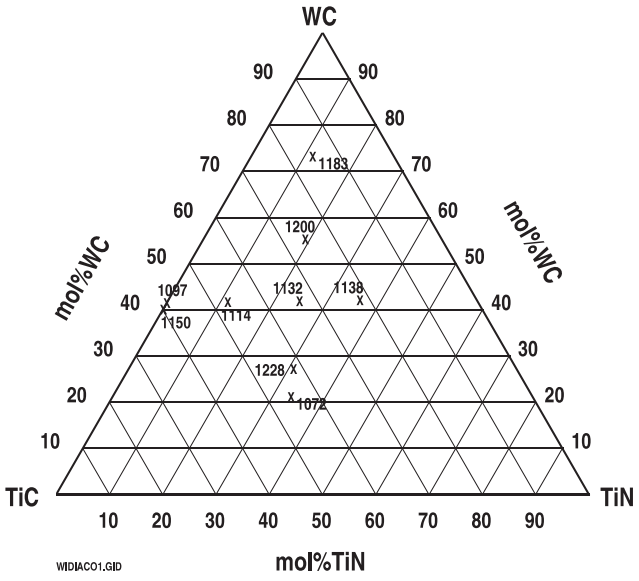

Fig. 9. Temperatures of the main CO peak of the WC–TiC–TiN–Co alloys.

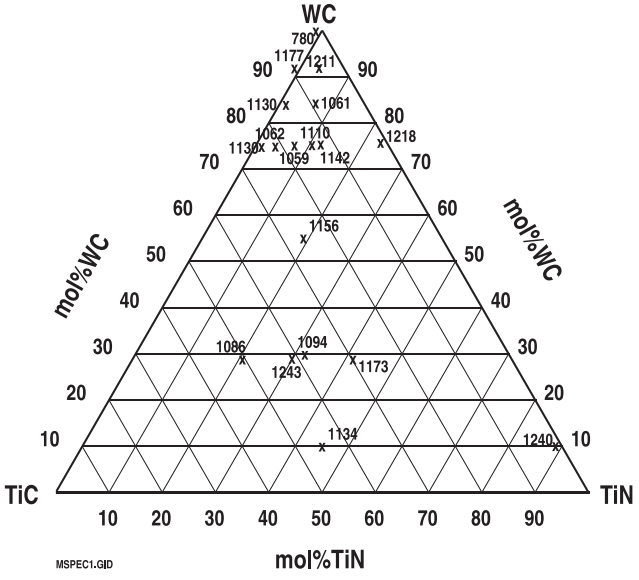

Fig. 10. Temperatures of the main CO peak of the WC–TiC–TiN–TaC/NbC–Co alloys.

phase. If the alloys contain hard phases of the binary system TiC–WC, the micro-structure is composed of faceted WC with large elongated grains and a spherical core-rim type (Ti, W)C with a Ti-rich core . An example of such micro-structure is given in Fig. 13.

As to nitrogen-containing hardmetal and cermets, TiN usually acts as a grain growth inhibitor and produces very fine-grained micro-structures with a spherical tungsten-rich phase. Generally, the grain size of the hard phases decreases with increasing N/(C + N) content of the alloy. Upon increase of the TiN content the WC-rich

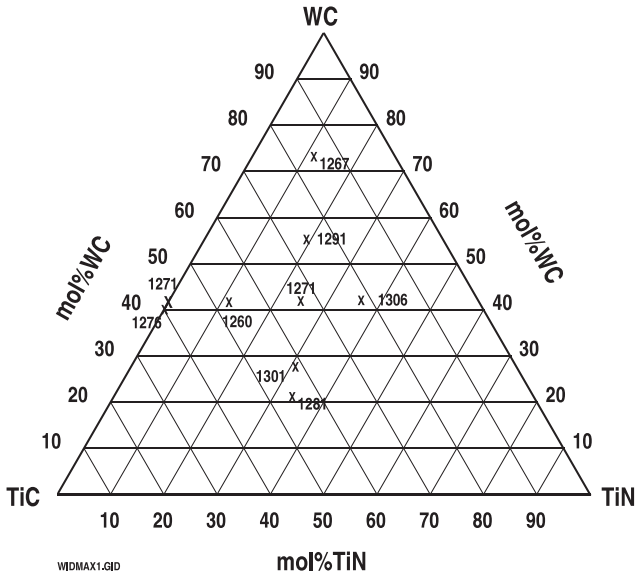

Fig. 11. Temperatures of the main N_2 peak of the WC–TiC–TiN–Co alloys.

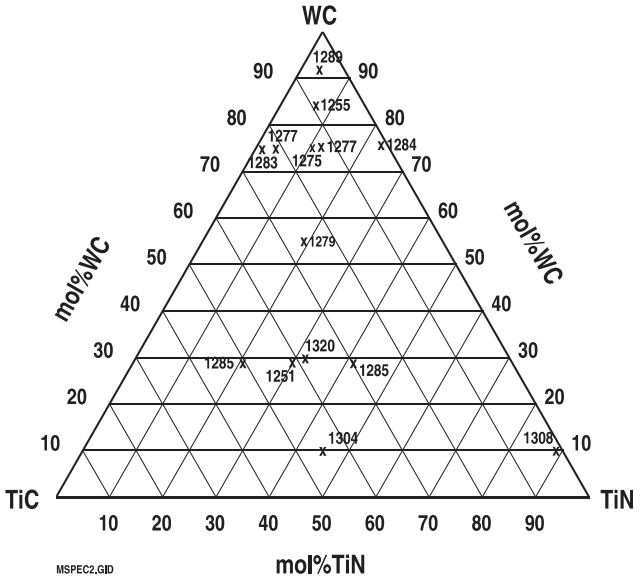

Fig. 12. Temperatures of the main N_2 peak of the WC–TiC–TiN–TaC/NbC–Co alloys.

(or pure WC) phase becomes much less faceted and the surface of the particles gets irregular with shape of these particles being spherical. The (Ti, W)(C, N) phase also has a ''core-rim'' type structure though, the individual grains can hardly be seen at low magnification. Moreover, the WC phase content in the micro-structure increases to maximum if the N/(C + N) ratio of the alloys increases. Fig. 14 gives an example of a N-containing alloys.

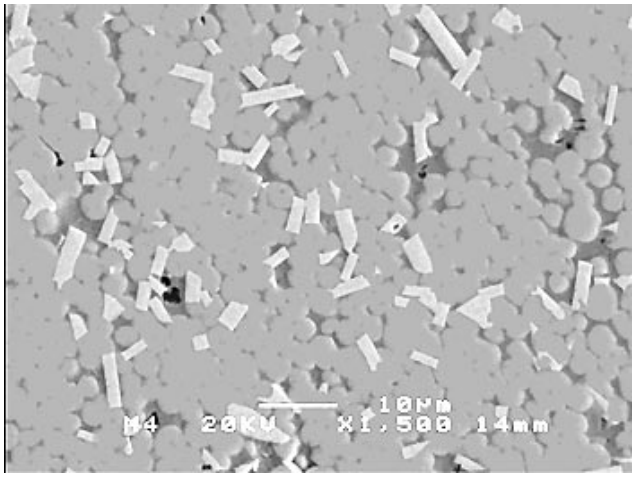

Fig. 13. SEM image of an alloy sample (WC/TiC = 42/58 in mol%; without nitrogen) Coarse-grained microstructure with faceted bright WC grains.

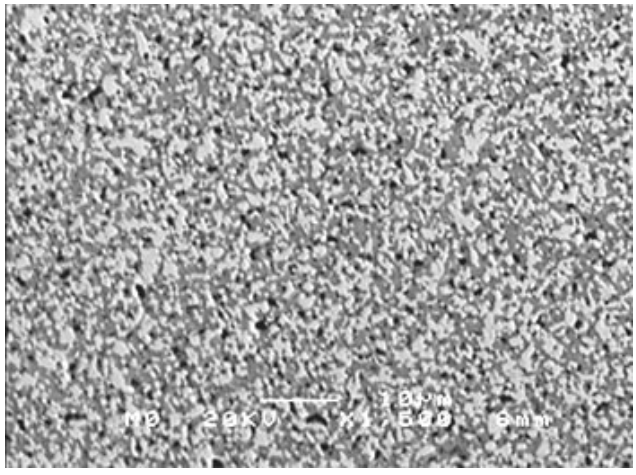

Fig. 14. SEM image of an alloy sample (WC/TiC/TiN = 55/25/20 in mol%). Fine-grained structure of both the WC-rich and TiC-rich phase.

3.6. New nitrogen-containing hardmetals and cermets

The results in the Sections 3.1 and 3.5 provide information about how to design new cutting tool materials and how to control the corresponding metallurgical reactions in order to prepare them. The sintering atmosphere should be controlled either to modify the sintered bodies before densification or to form the desired micro- and macro-structures on the surface of the compacts.

Three types of the new cutting tool materials CFL, FGM and M-FGM as well as their processing and the possible metallurgical mechanisms are schematically illustrated in Fig. 15. Through different atmosphere

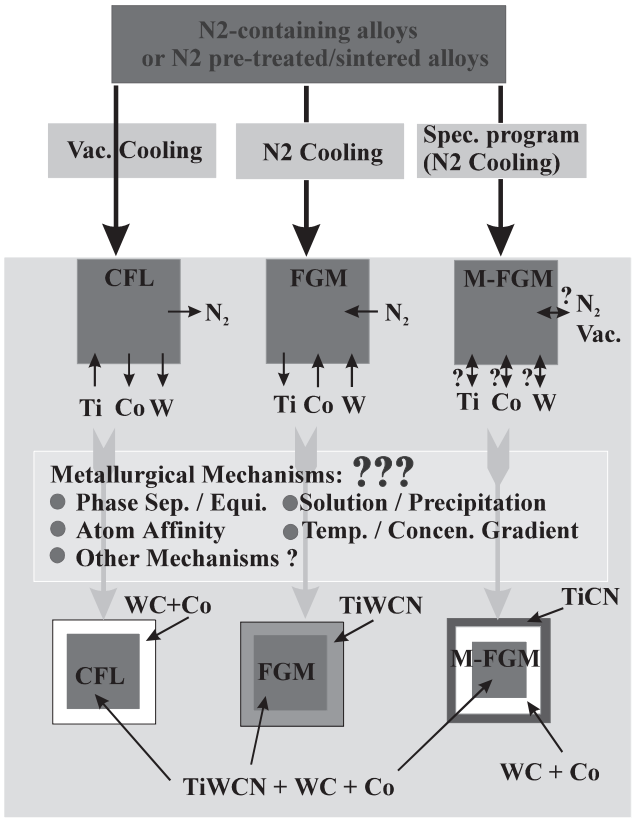

Fig. 15. Schematical illustration of the CFL, FGM and M-FGM new cutting materials and the corresponding processing to make the same.

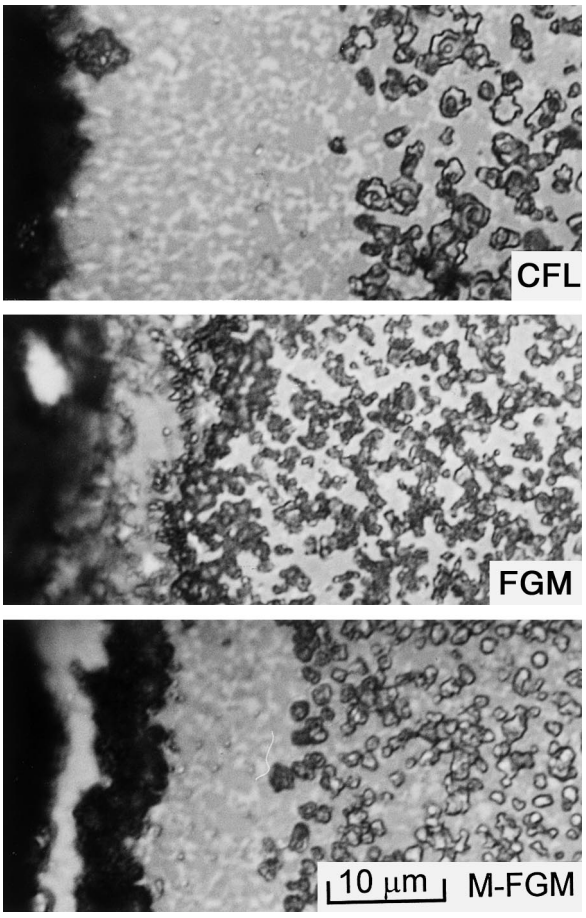

Fig. 16. Examples of the microstructures of CFL, FGM and M-FGM new cutting tool materials; magnification: 1350×.

treatments before and/or after densification, CFL, FGM and M-FGM can be prepared with hard phase covering most compositional range of the TiC–TiN–WC system. The composition of the starting materials can be either nitrogen-containing (Ti, W)(C, N) + Co/Ni powder mixtures, or non nitrogen-containing (Ti, W)C + Co/Ni powder compacts with nitrogen pre-treating.

The micro-structures of the CFL, FGM and M-FGM materials are given in Fig. 16. The CFL material consists of a cubic phase-free-layer (WC + Co/Ni) on the surface. As contrast to CFL, FGM material features a cubic-phase rich, WC phase-free surface layer which has compositional gradients of Ti, W, Co, C and N up to 500 μm, depending on the overall composition of the alloy. An example of a GDS depth analysis of a FGM alloy is shown in Fig. 17. The depth of the compositional gradient of this alloy is about 30 μm. M-FGM material has multi-FGM laminate layers and each layer has composition gradient. Fig. 18 gives an example of a GDS depth analysis of an M-FGM material.

In addition to CFL, FGM and M-FGM materials, a TiN-based material with hard phase composition of 90 mol% TiN–10 mol% WC has also been developed. By "state-of-the-art" industrial technology under modified sintering atmosphere, this kind of material could be

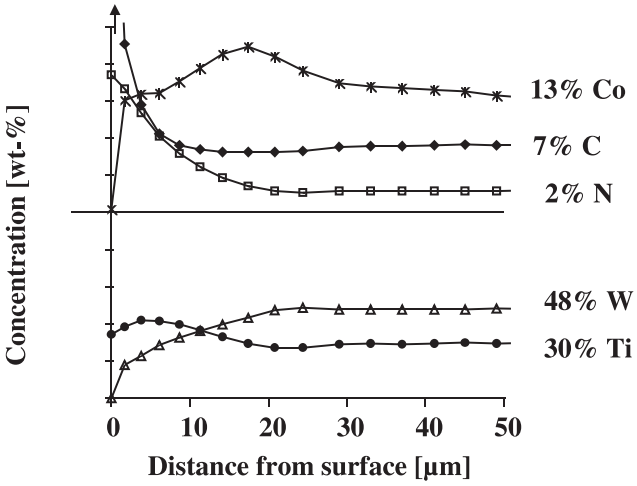

Fig. 17. An example of the GDS depth profile of a FGM sample.

sintered to full density (porosity < A02B00C00). Due to the self-lubricating property of TiN, this new material has potential for some special applications such as dry-cutting, drawing dies, etc.

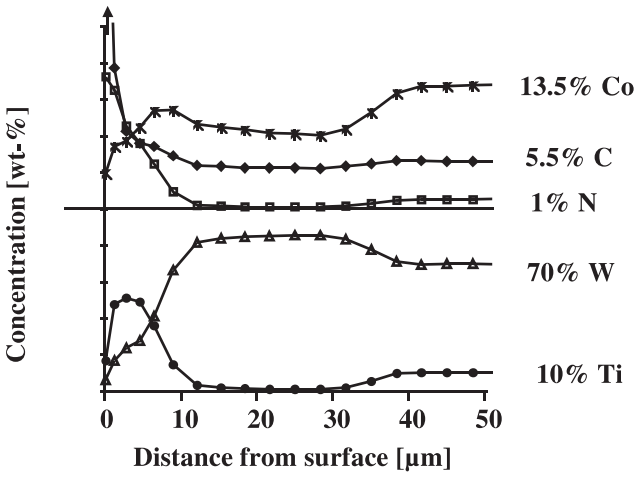

Fig. 18. An example of the GDS depth profile of an M-FGM sample.

4. Discussions

4.1. Phase separation/phase equilibria

The phase separation and phase equilibria in the Ti–W–C–N hard phase system were thought to cause different surface structures, because the solid solution of WC in TiCN depends on the nitrogen content of the (Ti, W)(C, N). The higher the nitrogen content in the hard phase, the lower the solution of the WC in the (Ti, W)(C, N). Since any variation of atmosphere in equilibrium with the (Ti, W)(C, N) can change the corresponding nitrogen content of the hard phase, the formation of CFL, FGM and M-FGM depends greatly on the sintering atmosphere.

4.2. Atom affinity

The atom affinity between Ti and N is much stronger than that between W and N. If the (Ti, W)(C, N) hard phase is treated at high temperature under different atmosphere, for instead under vacuum, a nitrogen gradient (N-poor surface) will be produced because of denitrification of the (Ti, W)(C, N). Therefore, Ti atoms will move inwards against the high nitrogen potential of the matrix. A CFL (cubic-free layer) surface will form due to the inward movement of Ti. The enrichment of Co is however not explained by such a mechanism.

4.3. Solution/precipitation

The solution/precipitation through liquid phase during heating/cooling process might play a very important role. The movement (diffusion) of Ti, W, C and N through Co melt might be much easier and faster than through solid phase.

4.4. Temperature/concentration gradient

There exist temperature gradients of melting/solidifying points in the TiC–TiC–TiN–Co system. During sintering of (Ti, W)(C, N)–Co powder compacts, a temperature gradient between sample surface and matrix can be established because of the Ti, W, C and N movement (diffusion) forced by atmosphere. For alloys with original compositions located in the three-phase region, i.e. WC + (Ti, W)(C, N) + Co region, such movement, (e.g. if under N_2 atmosphere) can move the composition of the sample surface into the two-phase region, i.e. (Ti, W)(C, N) + Co region. Therefore, WC will disappear in the surface zone. Moreover, the temperature gradient can also result in the Co gradient near the surface zone.

5. Outlook

Nearly three decades have passed since nitrogen-containing cermets first came into being. Nowadays, nitrogen-containing hardmetals such as modern cermets and CFL substrates for coated inserts have been widely used in industry. New knowledge about phase equilibria, metallurgical reactions of WC–TiC–TiN–, WC–TiC–TiN–Co– and WC–TiCN–TaC/NbC–Co/Ni–alloys leads to the latest advances in FGM and M-FGM cutting tool materials. Due to the distinctive micro- and macro-structures, FGM and M-FGM materials are believed to have the potential to successfully compete with or even be superior to conventional coated hardmetals.

References

[1] Ettmayer P, Lengauer W. The story of cermets. Powder Metall Int 1989;21(2):37–8.
[2] Pastor H. Titanium-carbonitride-based hard alloys for cutting tools. Mater Sci Eng A 1988;105/106:401–9.
[3] Ettmayer P, Kolaska H, Dreyer K. Effect of the sintering atmosphere on the properties of cermets. Powder Metall Int 1991;23(4):224–9.
[4] Ettmayer P, Kolaska H, Lengauer W, Dreyer K. Ti(C, N) cermets – metallurgy and properties. Int J Refract Met & Hard Mater 1995;13:343.
[5] Suzuki H, Hayashi K, Taniguchi Y. The β-free layer near the surface of vacuum-sintered WC–β-Co alloys containing nitrogen. Trans Japan Inst Met 1981;22(11):758–64.
[6] Yohe WC. The development of cubic-carbide-free surface layers in cemented carbides without nitrogen. In: Bildstein H, Eck R, editors. Proceedings of the 13th International Plansee Seminar, Metallwerk plansee, vol. 2, 1993, p. 151–68.
[7] Schwarzkopf M, Exner HE, Fischmeister HF. Kinetics of compositional modification of (W, Ti)C–WC–Co alloy surfaces. Mater Sci Eng A 1988;105/106:225–31.

[8] Tsuda K, Ikegaya A, Isobe K, Kitagawa N, Nomura T. Development of functionally graded sintered hard materials. Powder Metall 1996;39(4):296–300.

[9] Chen L, Lengauer W. Metallurgical mechanisms and processing technologies of FGM (Ti, W)(C, N)–Co hardmetals. Internal reports of Austrian Research Center, OEFZS-A–4516, Nov. 1998; OEFZS-A–4185, Sept. 1997.

[10] Lengauer W, Chen L, Garcia J, Ucakar V, Dreyer K, Kassel D, Daub HW. Diffusion-controlled surface modification for fabrication of functional-gradient (Ti, W)C based cemented carbonitrides. Proceedings of PM^{2}TEC'99 International Conference on Powder Metallurgy and Particulate Materials.